ELSEVIER

Journal of Chromatography A, 867 (2000) 23–43

JOURNAL OF CHROMATOGRAPHY A

www.elsevier.com/locate/chroma

# Simultaneous optimization of the analysis time and the concentration detectability in open-tubular liquid chromatography

Gert Desmet*, Gino V. Baron

*Vrije Universiteit Brussel, Department of Chemical Engineering, Pleinlaan 2, 1050 Brussels, Belgium*

Received 26 August 1999; received in revised form 1 October 1999; accepted 14 October 1999

**Abstract**

Scott's OT-LC minimal analysis time problem has been solved analytically and has been extended to thick-film and/or large diameter columns. The optimisation analysis has also been applied to a number of relative performance indexes ($C_{max}/t_{anal}$, $C_{max}$.d$/t_{anal}$ and $C_{max}.u.$d$^2/t_{anal}$) which provide a quantitative insight on the extent to which OT-LC allows to combine short analysis times with a large concentration detectability. 

*Keywords:* Optimization; Analysis time; Concentration detectability

## 1. Introduction

Whereas capillary GC has nearly completely outstripped its packed column variant, the situation in LC is completely the opposite: the commercial success of OT-LC lags far behind that of HPLC. This is mainly due to the small molecular diffusivity in liquids: to obtain comparable separation speeds, the diameter ($d$) of OT-LC columns should be of about the same size as the micron particles typically employed in HPLC [1,2]. Apart from the problems arising from the need for miniaturised (on-column) injection and detection systems [3,4], such narrow columns inevitably have a very small mass loadability and a correspondingly small concentration detectability [5,6]. To alleviate this problem, a lot of research efforts [7–9] have been directed towards the increase of the surface area and the thickness ($\delta$) of the stationary phase. However, and apart from the practical coating problems [6,10,11], $\delta$ is of course also limited by restrictions on the analysis time. Finding a suitable compromise between the analysis time and the concentration detectability is a difficult problem which requires a careful compromise on the values of the design parameters $d$, $\delta$ and $k'$ [12,13]. To increase the insight in the complex and strongly inter-coupled relation between these design variables and the resulting resolution, analysis time and concentration detectability, the present paper reports on a systematic mathematical analysis of the theoretical expressions for the analysis time and the concentration detectability in OT-LC.

First, the pure analysis time minimisation problem is considered (Section 3). This problem has already been addressed by Scott [14] for small $\delta$ and for $d=d_{opt}$, but it has not been considered yet for columns with a large mass loadability, i.e. for columns with a large, non-optimal diameter and/or with a large stationary film thickness. As has already been pointed out by Poppe and Kraak [15], the

*Corresponding author. Tel.: +32-2-629-32-51; fax: +32-2-629-32-48.

*E-mail address:* gedesmet@vub.ac.be (G. Desmet)

0021-9673/00/$ – see front matter 
PII: S0021-9673(99)01102-4

typical diffusion rates in liquid–liquid chromatography allow to envision phase volume ratio's ($m$) of the order of unity without leading to an excessive increase of the analysis time. This point will now be investigated under fully optimised $k'$-conditions, but also by accounting for the undesirable thick-film diffusion effects which occur when $\phi = \delta/d > 0.1$ [16]. In the second part of the paper, the optimisation analysis is extended to a number of relative performance criteria in which the need for concentrated, easily detectable peaks is balanced against the requirement of a short analysis time ($C_{max}/t_{anal}$, $C_{max}.d/t_{anal}$, $C_{max}.u.d^2/t_{anal}$). A complete survey of all existing analytical solutions is made (Sections 4–6), and the resulting optimal operating conditions are discussed (Section 7). The influence of the stationary phase diffusivity, represented by the parameter $\varepsilon$ ($=D_s/D_m$), is considered as well.

Unless otherwise stated, all presented graphs are for $\alpha_s = 1.01$, $R_s = 1.25$, $D_m = 1.10^{-9}$ m$^2$/s and $\mu = 10^{-3}$ kg/(m.s). The mobile phase velocity has always been adjusted such that the pressure drop exactly equals $\Delta P = 200$ bar. In all the graphs, the presently proposed analytical expressions are plotted together with the results of a conventional numerical optimisation study. The fact that both approaches yield completely overlapping curves validates the analytical calculations.

## 2. Theoretical chromatographic equations and performance characteristics

All calculations in the present study are based upon the well-established theoretical equations for the resolution ($R_s$), the HETP and the pressure drop ($\Delta P$):

$$R_s = \frac{\alpha_s - 1}{4} \cdot \sqrt{N} \cdot \frac{k'}{(1+k')} \tag{1}$$

$$\text{HETP} = \frac{2D_m}{u} + 2uC \tag{2}$$

$$\Delta P = \frac{32\mu u N \text{HETP}}{d^2} \tag{3}$$

The retention factor $k'$ in Eq. (1) has been taken as the product of the phase volume ratio ($m$) and the distribution coefficient $K_1$ of the first eluting component of a given critical pair ($k' = mK_1$). For a cylindrical capillary, $m$ is given by:

$$m = 4\phi + 4\phi^2 \tag{4}$$

The $C$-factor in Eq. (2) consists of two terms, respectively representing the mobile phase ($C_m$) and the stationary phase ($C_s$) mass transfer resistance:

$$C = C_m + C_s = (C'_m + C'_s) \cdot \frac{d^2}{(1+k')^2 D_m} \tag{5a}$$

with:

$$C'_m = \frac{1 + 6k' + 11k'^2}{192} \tag{5b}$$

and

$$C'_s = \frac{k'}{\varepsilon} \cdot Z, \text{ with:}$$

$$Z = \frac{1}{32} \cdot \left[ \frac{(1+2\phi)^4 \ln(1+2\phi)}{\phi(1+\phi)} - 12\phi(1+\phi) - 2 \right] \tag{5c}$$

Eq. (5c) represents the extended Aris-solution [17] for the stationary phase mass transfer. Whereas the more commonly used Golay-solution (cf. Eq. (5d)) is restricted to so-called thin-film columns, the Aris-solution (Eq. (5c)) also accounts for the undesirable radial diffusion effects which become apparent when the film becomes so thick that it can no longer be regarded as a flat slab layer [16]. In view of the present trend towards phase thickness ratio's in excess of $\phi = 0.1$ [7,9,10,18], and in order to maintain a general approach, all the calculations in the present study are based upon Eq. (5c). It can however easily be verified that Eq. (5c) reduces to Golay's thin-film expression when $\phi < 0.1$:

$$Z \cong Z_{tf} = \phi^2/3 \tag{5d}$$

Throughout the text, the full Aris-solution and the thin-film solution are continuously compared. This allows to clearly delimit the range of validity of the thin-film approximation.

Combining Eqs. (1–3), the mobile phase velocity $u$ which can maximally be applied when a given separation quality has to be achieved in a column with a given diameter and with a given maximal allowable pressure drop can be written as:

$$u = \sqrt{\frac{1}{C} \cdot \left( \frac{\Delta P d^2}{64 \mu N} - D_m \right)}$$
$$= \sqrt{\frac{D_m}{C} \cdot \left( \theta \frac{k'^2}{(1+k')^2} - 1 \right)}, \tag{6a}$$

with:

$$\theta = \frac{\Delta P (\alpha_s - 1)^2}{1024 R_s^2 \mu D_m} \cdot d^2 \tag{6b}$$

Eq. (6) shows the natural emergence of a dimensionless number ($\theta$), which will be used throughout the present paper to represent the influence of $d$ for all possible combinations of $\Delta P$, $\mu$, $D_m$, $R_s$, $\alpha_s$ in a condensed manner.

The two most important performance characteristics considered in the present study are the analysis time ($t_{anal}$) and the peak solute concentration ($C_{max}$):

$$t_{anal} = \frac{N.\mathrm{HETP}}{u} \cdot (1 + k') \tag{7}$$

$$C_{max} = \frac{m_{30} \rho_{sf}}{\mathrm{MW}} \cdot \frac{1+k'}{k'^2} \cdot \frac{m}{\sqrt{2\pi N}} \tag{8}$$

The expression for $C_{max}$ has been taken from Tock et al. [13,19]. Using Eqs. (1–3), and (6), it can easily be verified that Eq. (7) can be written as:

$$t_{anal} = 1024 \cdot \frac{\mu}{\Delta P} \cdot \frac{R_s{}^4}{(\alpha_s - 1)^4} \cdot \Gamma \tag{9a}$$

with:

$$\Gamma = (C'_m + C'_s) \cdot \frac{\theta^2 (1+k')}{\theta k'^2 - (1+k')^2} \tag{9b}$$

As will become clear, the expression for $t_{anal}$ now has a form which is suitable to perform the desired optimisation study: the expression is divided into an optimizable part, $\Gamma$, containing the design parameters $d$, $k'$ and $\phi$, and a non-optimizable part, containing the parameters $\mu$, $\Delta P$, $R_s$ and $\alpha_s$. Replacing $N$ via Eq. (1), the $C_{max}$-expression in Eq. (8) can also be separated into a non-optimizable part ($A$) and an optimizable part ($m/k'$):

$$C_{max} = \frac{m_{30} \rho_{sf}}{\mathrm{MW}} \cdot \frac{1}{\sqrt{2\pi}} \cdot \frac{(\alpha_s - 1)}{4.R_s} \cdot \frac{m}{k'} = A \cdot \frac{m}{k'} \tag{10}$$

It should be noted that by consistently replacing $N$ by its relation to $R_s$, $\alpha_s$ and $k'$, all optimisations in the present study are performed on the basis of an equal resolution instead of on the basis of equal theoretical plate numbers. This approach avoids any a priori assumptions on the value of $k'$, $N$ or the column length.

## 3. Optimising for a minimum analysis time

### *3.1. Optimising the film thickness ratio $\phi$ (d and k′ are freely selectable constants)*

Minimising $\Gamma$ (see Eq. (9b)) with respect to $\phi$ yields the trivial solution:

$$\frac{\partial \Gamma}{\partial \phi} = \frac{\partial C'_s}{\partial \phi} = 0 \Leftrightarrow \phi = 0 \tag{11}$$

This condition is of course very unfavourable from the mass loadability point of view.

### *3.2. Optimising the column diameter d ($\phi$ and k′ are freely selectable constants)*

As $\partial \Gamma / \partial d = 0$ corresponds to $\partial \Gamma / \partial \theta = 0$ (Eq. (6b)), the optimal column diameter is given by:

$$\frac{\partial \Gamma}{\partial \theta} = 0 \Leftrightarrow \theta \frac{k'^2}{(1+k')^2} = 2 \quad \text{or:}$$

$$\theta_{opt} = 2 \frac{(1+k')^2}{k'^2} \tag{12}$$

Introducing this result into Eq. (6a), it follows directly that the mobile phase velocity under $\theta = \theta_{opt}$-conditions is given by:

$$u = \sqrt{\frac{D_m}{C}} \tag{13}$$

This value is exactly equal to the $u = u_{opt}$-velocity [20] marking the minimum of the (HETP,$u$)-relationship. Eq. (13) hence provides a direct analytical proof for the heuristic reasoning of Knox and Saleem [21,22], which has thus far only been confirmed numerically [20,23]. Replacing $\theta$ by its definition in Eq. (6b), and reintroducing the expression for $N$, it can easily be verified that Eq. (12) in fact corresponds to Giddings' $d_{\mathrm{opt}}$-expression [24]:

$$d_{\mathrm{opt}}=\sqrt{\frac{128\mu ND_{\mathrm{m}}}{\Delta P}} \tag{14}$$

Combining Eq. (14) with Eqs. (1) and (6b), it can easily be noted that the $\theta.k'^2/(1+k')^2$-group which appears in Eq. (6a) can also be written as:

$$\theta\,\frac{k'^2}{(1+k')^2}=2\cdot\frac{d^2}{d_{\mathrm{opt}}{}^2}, \tag{15}$$

showing that the $\theta$-number can be interpreted as the square of the number of times a given column diameter is smaller or larger than $d_{\mathrm{opt}}$. The $\theta$-number can also be interpreted in terms of Giddings' [24] critical pressure drop. According to the present analysis, this critical pressure drop corresponds to the existence of a minimum $\theta$-value, arising from the fact that the expression under the square-root sign of Eq. (6a) should be strictly positive. From Eq. (6a), it follows directly that this restriction is given by:

$$\theta>\frac{(1+k')^2}{k'^2} \tag{16}$$

### 3.3. Optimising the column retention factor $k'$ ($d$ and $\phi$ are freely selectable constants)

Optimising $\Gamma$ with respect to $k'$, the following 4th order equation in $k'$ is obtained:

$$-(5+F)-2(6+\theta+F)k'-[60+7\theta+F(1+\theta)]k'^2-44k'^3+11(\theta-1)k'^4=0, \tag{17}$$

with:

$$F=192Z/\varepsilon \tag{18}$$

Eq. (17) can be used to directly calculate $k'_{\mathrm{opt}}$ for all $d$, $\phi$ and $\varepsilon$. As Eq. (17) is of 4th order, it can be solved analytically [25]. The resulting expression is however very complex. It is in fact easier to calculate $k'_{\mathrm{opt}}$ directly from Eq. (17) using a numerical root-finding routine. Doing so, attention should be paid to the fact that the range of feasible $k'$-values has a sub-limit ($k'_{\min}$). As $\theta$ should always be larger than 1 (let $k'$ vary between 0 and $\infty$ in Eq. (16)), it can easily be verified from Eq. (16) that:

$$k'_{\min}=\frac{1+\sqrt{\theta}}{\theta-1} \tag{19}$$

### 3.4. Simultaneously optimising $\phi$ and $k'$ ($d$ is a freely selectable constant)

A special case of Eq. (17) arises for $\phi\to0$, representing the simultaneous optimisation of $\phi$ and $k'$. In this case, all the terms in $F$ vanish. The equation however remains of 4th order and the derivation of an analytical solution remains very cumbersome.

### 3.5. Simultaneously optimising $d$ and $k'$ ($\phi$ is a freely selectable constant)

Considering all possible $k'$-values with their corresponding $d_{\mathrm{opt}}$-value, Scott has shown numerically [14] that there exists a given $k'$-value for which the analysis time is absolutely minimal. The present analysis allows to establish an analytical proof for this. Putting $\theta=\theta_{\mathrm{opt}}=2(1+k')^2/k'^2$ in Eq. (17), and dividing the result by $(1+k')^2$, yields:

$$-4-(19+3F)k'-22k'^2+11k'^3=0 \tag{20}$$

Eq. (20) holds for all possible values of $\phi$. As it is of 3rd order, it can be solved according to Appendix A, with $a_2$, $p$ and $q$ given by:

$$a_2=-2,\ p=-\frac{101+9F}{99}\quad\text{and}\quad q=-\frac{313+27F}{297} \tag{21}$$

With $p$ and $q$ known, a discriminant $R$ can be calculated (Eq. (A.4)). For small $F$, $R>0$ and Eq. (20) has one real root (Eq. (A.5)). For large $F$, $R<0$ and Eq. (20) has three real roots, obtained by, respectively, putting $n=0$, 1, or 2 in Eq. (A.6). Considering for example the limiting case of $\phi\to0$ (put $F=0$ in Eq. (21)), $R>0$ and Eq. (A.5) yields:

$$k'_{\mathrm{opt}}=2.69\quad(\phi\to0\text{-case}) \tag{22}$$

Eq. (22) constitutes an exact validation for Scott's numerical result ($k'_{\mathrm{opt}}=2.7$, [14]). By replacing the factors 6, 11 and 192 by, respectively, 9, 51/2 and

210 in Eq. (5b), and by replacing the factor 32 by 12 in Eq. (3), the above analysis can be repeated for columns with a flat rectangular cross-section, yielding $k'_{opt}=2.47$.

Fig. 1a clearly shows that the Scott-solution ($k'_{opt}=2.69$) no longer holds for large mass loadability columns: $k'_{opt}$ strongly increases with $\phi$ when $\phi>0.1$. With the present analysis, the exact $k'_{opt}$-values in this range can now be directly obtained from Eq. (20). Whereas the $k'_{opt}$-curves in Fig. 1a strongly depend upon $\varepsilon$, a perfectly unified plot is obtained when plotting the $k'_{opt}$-values versus the ratio of $C_s$ to $C$ (Fig. 1b). Fig. 1b can hence be used to directly read out $k'_{opt}$ for all possible combinations of $\phi$ and $\varepsilon$. In Fig. 1c, the importance of separating a critical pair at the $k'_{opt}$-values given by Eq. (20) is investigated by comparing the analysis time for $k'=2.69$ to the analysis time for $k'=k'_{opt}$ (Fig. 1c). It can clearly be noted that, depending on the value of $\varepsilon$, a difference of up to 100% is obtained in the range of $0.1<\phi<1$, which is precisely the range of interest of the present study. Fig. 1d clearly shows that when $\varepsilon=0.5$, the film thickness can be increased until $\phi=0.5$ before this leads to a doubling of $t_{anal}$ (cf. dashed line). As $\phi=0.5$ corresponds to $m=3$, it is hence obvious that phase volume ratio's of the order of 1 to 3 are perfectly feasible in OT–LC, provided that suitable coating methods can be developed. This confirms an early statement by Poppe and Kraak [15]. As the data in Fig. 1d are for the full Aris-solution, it has now been demonstrated that this statement still holds when accounting for the unfavourable thick-film diffusion effect. The value of $m=3$ taken from Fig. 1d is even larger than the value of $m=1$ put forward in Ref. [15]. This is due to the fact that the data in Fig. 1d refer to the fully optimised case (i.e., $k'=k'_{opt}$ given by Eq. (20)).

Taking Eq. (14), and inserting the $k'_{opt}$-values determined by Eq. (20), the fully optimised column diameter ($d^*_{opt}$), i.e., the diameter yielding the smallest possible analysis time for a given value of $\alpha_s$ and $R_s$, is obtained:

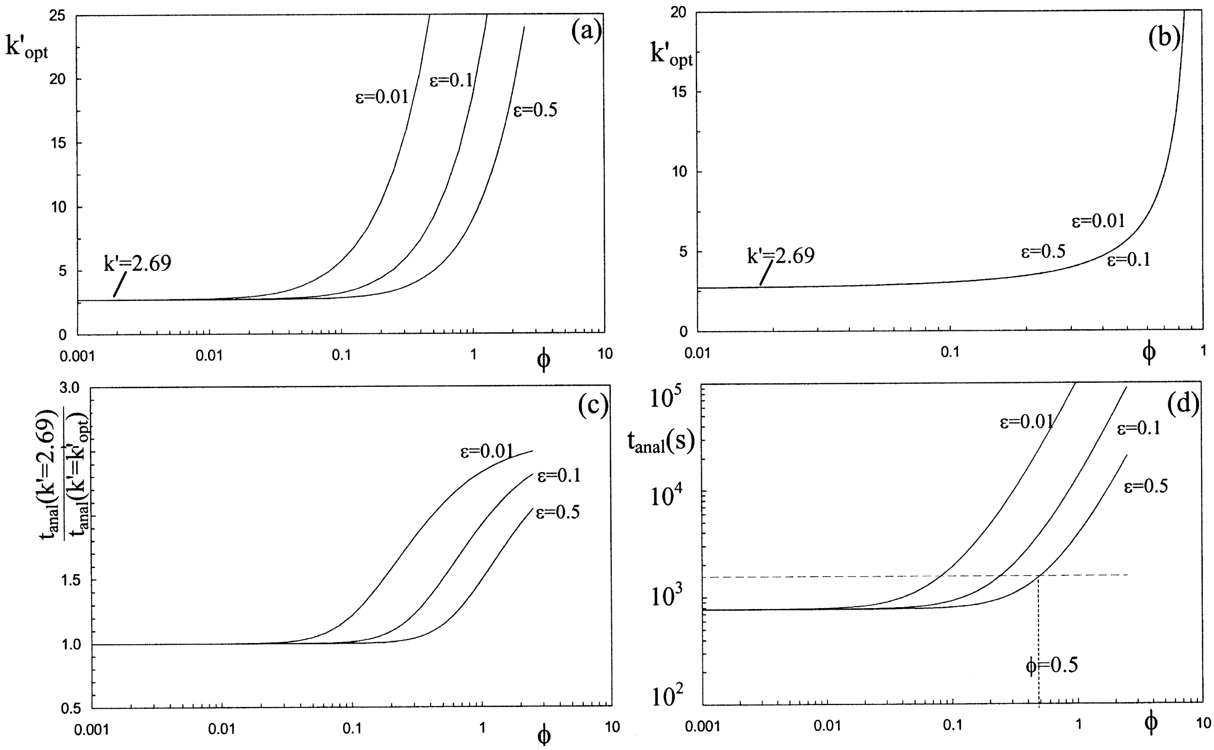


Fig. 1. (a) Minimal $t_{anal}$-problem: variation of $k'_{opt}$ with $\phi$ for three different values of $\varepsilon$ ($d=d_{opt}$-case). (b) Representation of the $k'_{opt}$-data of (a) as a function of $C_s/C$. (c) Ratio of $t_{anal}(k'=2.69)$ to $t_{anal}(k'=k'_{opt})$ versus $\phi$. (d) $t_{anal}$ versus $\phi$ for the $k'_{opt}$-data represented in (a)–(b).

$$d^{*}_{opt} = \sqrt{128 \cdot \frac{16(\alpha_s - 1)^2}{{R_s}^2} \cdot \frac{(1 + k'_{opt})^2}{{k'_{opt}}^2} \cdot \frac{\mu D_m}{\Delta P}} \quad (23)$$

It should be noted that, as $k'_{opt}$ depends upon both $\phi$ and $\varepsilon$, the $d^{*}_{opt}$-value also depends upon $\phi$ and $\varepsilon$ The larger $\phi$, or the smaller $\varepsilon$, the larger the value of $k'_{opt}$ (cf. Fig. 1a), and the smaller the value of $d^{*}_{opt}$.

### *3.6. Optimising the column retention factor $k'$ when $d \gg d_{opt}$*

With the present detector technology, the $d = d_{opt}$-optimisation presented in Sections 3.2 and 3.5 is however not very practically useful. Whereas $d_{opt}$ for a typical routine analysis requiring less than 100 000 plates is of the order of 1 μm or even below, the poor sensitivity of LC detectors typically limits the present state-of-the-art to columns of about 5 μm [6]. The calculation of $k'_{opt}$ for columns with a diameter which is (much) larger than $d_{opt}$ is therefore of a more practical importance. Due to the derivation in Section 3.3, this now simply comes down to solving Eq. (17) with the appropriate $\theta$-value. The results are plotted in Fig. 2, showing that $k'_{opt}$ continuously decreases with increasing $d$ for a given value of $\phi$ and $\varepsilon$. It can also be noted that $k'_{opt}$ increases with increasing $\phi$ for a given value of $d$ (or $\theta$). It has also been verified that, for a given value of $\phi$, $k'_{opt}$ increases with decreasing $\varepsilon$. Fig. 2 also shows that the $k'_{opt}$-values reach a limiting value for $\theta > 100$. Considering a 5 μm column, with $D_m = 1.10^{-9}$ m$^2$/s, $\Delta P = 200$ bar, $\mu = 1.10^{-3}$ kg/(m.s) and $R_s = 1.25$, Eq. (6b) shows that $\theta > 100$ for all $\alpha_s > 1.018$. The $\theta = \infty$-limit is hence representative for most present OT-LC applications. Putting $\theta = \infty$, Eq. (17) becomes:

$$2 + (7 + F)k' - 11k'^3 = 0 \quad (24)$$

As Eq. (24) is of 3rd order, it can be solved according to the Appendix, with:

$$a_2 = 0,\ p = -(7 + F)/33 \quad \text{and}$$
$$mq = -1/11 \quad (25)$$

For all $F$, the positive real root of Eq. (24) is given by Eq. (A.6) with $n = 0$. Fig. 2 clearly shows that, although Eq. (24) is strict mathematically only valid when $\theta = \infty$, it provides an excellent approximation for the exact $k'_{opt}$-values from $\theta = 100$ on. Considering for example the $\phi \rightarrow 0$-limit, $F$ can be put to zero in Eq. (25), and Eq. (A.6) yields $k'_{opt} = 0.914$ (cf. Fig. 2). From Eq. (25), it can easily be verified that the $k'_{opt} = 0.914$-result is a sufficiently close approximation for all combinations of $\phi$ and $\varepsilon$ for which $F \ll 7$.

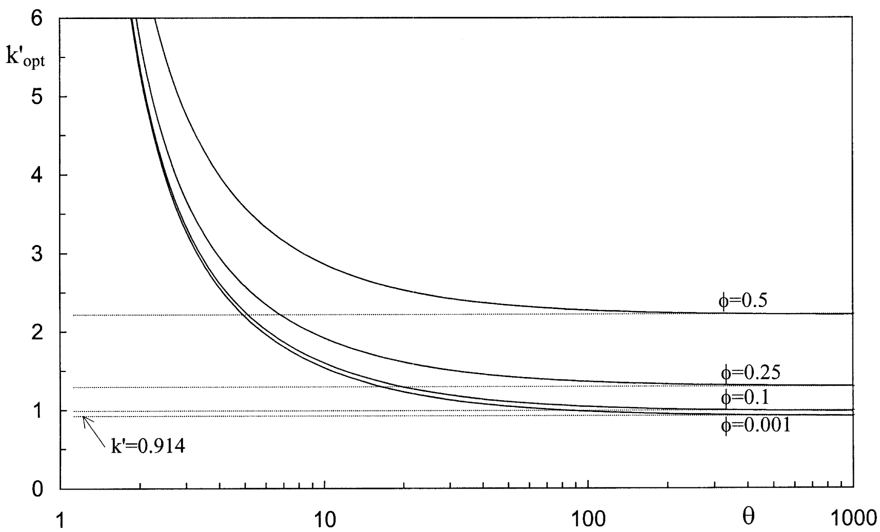


Fig. 2. $k'_{opt}$ vs. $\theta$ for four different values of $\phi$ ($\varepsilon = 0.5$) The dashed lines refer to the $\theta = \infty$-limit solution given by Eq. (24).

## 4. Simultaneous optimisation of $C_{max}$ and $t_{anal}$

From Eqs. (9) and (10), the ratio of $C_{max}$ to $t_{anal}$ can be written as:

$$\frac{C_{max}}{t_{anal}}=\frac{m_{30}\rho_{sf}}{MW}\cdot\frac{1}{\sqrt{2\pi}}\cdot\frac{\Delta P}{32\mu}\cdot\frac{(\alpha-1)^5}{64^2R_s^{\;5}}\cdot\frac{m}{k'}\cdot\frac{1}{C'_m+C'_s}\cdot\frac{\theta k'^2-(1+k')^2}{\theta^2(1+k')} \tag{26}$$

From Eq. (26), it can easily be noted that the optimisation procedure adopted in Section 3 can also be applied to $C_{max}/t_{anal}$. Performing this optimisation analysis is a useful exercise, because the $C_{max}/t_{anal}$-ratio is a measure for the ability of a column to generate concentrated, easily detectable peaks in a short time. Separating Eq. (26) into an optimisable and a non-optimisable part, the following goal function ($\Gamma$) is obtained:

$$\Gamma=\frac{m}{k'(1+k')}\cdot\frac{\theta k'^2-(1+k')^2}{(C'_m+C'_s)\theta^2} \tag{27}$$

### *4.1. Optimising the column diameter d ($\phi$ and $k'$ are freely selectable constants)*

As $C_{max}$ does not depend upon $\theta$, it is obvious that the goal function in Eq. (27) has the same $\theta$-dependency as the goal function in Section 3. The $d_{opt}$-value for the $C_{max}/t_{anal}$-optimisation is hence also given by $\theta_{opt}=2.(1+k')^2/k'^2$, and the optimal mobile phase velocity remains given by Eq. (13).

### *4.2. Optimising the column retention factor $k'$ (d and $\phi$ are freely selectable constants)*

Maximising the goal function in Eq. (27) with respect to $k'$ yields:

$$1+2(7+F)k'+(64+\theta+5F)k'^2+4(28+F)k'^3+[83-17\theta+(1-\theta)F]k'^4+22(1-\theta)k'^5=0 \tag{28}$$

As Eq. (28) is of 5th order, an analytical solution does not exist [25]. When accounting for Eq. (19), $k'_{opt}$ can however easily be found numerically.

### *4.3. Optimising the column retention factor $k'$ when $d \gg d_{opt}$*

As for Eq. (17), a special case of Eq. (28) is obtained for its $\theta=\infty$-limit. Putting $\theta=\infty$, Eq. (28) reduces to:

$$1-(17+F)k'^2-22k'^3=0 \tag{29}$$

This is a 3rd order equation, which can be solved according to the Appendix. It can be verified that the positive real root of Eq. (29) is given by Eq. (A.6), with either $n=0$, 1 or 2 (depending on the value of $F$). It was found that, for all $F$, Eq. (29) provides a sufficient approximation for all $\theta>100$. The $F=0$-solution is given in Section 7.

### *4.4. Simultaneously optimising d and $k'$ ($\phi$ is a freely selectable constant)*

Putting $\theta=\theta_{opt}=2.(1+k')^2/k'^2$ in Eq. (28), and dividing the obtained polynome by $(1+k')^2$, the following 3rd order equation in $k'$ is obtained:

$$3+2(6+F)k'+(5-F)k'^2-22k'^3=0 \tag{30}$$

Eq. (30) is valid for all $\phi$, and can be solved according to the Appendix. For small $F$, $R$ is positive and Eq. (A.5) applies. When $F$ is large, Eq. (A.6) applies. The thus obtained $k'_{opt}$-value should then be inserted into Eq. (23) to find the corresponding $d_{opt}$-value.

### *4.5. Optimising the film thickness ratio $\phi$ (d and $k'$ are freely selectable constants)*

Maximising $\Gamma$ with respect to $\phi$ yields:

$$\frac{\partial\Gamma}{\partial\phi}=0\Leftrightarrow\left[\frac{1+6k'+11k'^2}{192}+k'\frac{Z}{\varepsilon}\right]\cdot(1+2\phi)=\phi(1+\phi)\cdot\frac{k'}{\varepsilon}\cdot\frac{dZ}{d\phi} \tag{31}$$

Considering the full Aris-expression for $Z$, Eq. (31) cannot be solved analytically because of the presence of a logarithm. Adopting the double thin-film approximation ($Z\cong Z_{tf}=\phi^2/3$ and $m\cong 4\phi$), an analytical solution can however easily be obtained. Using this approximation, Eq. (31) becomes:

$$\phi = \phi_{opt} \Leftrightarrow \frac{1 + 6k' + 11k'^2}{192} + k'\,\frac{\phi^2}{3\varepsilon} = 2k' \cdot \frac{\phi^2}{3\varepsilon} \tag{32}$$

Or:

$$\phi_{opt} = \sqrt{3 \cdot \frac{1 + 6k' + 11k'^2}{192k'} \cdot \varepsilon} \tag{33}$$

Eq. (33) is valid for all $d$ and $k'$. Although it is a very simple expression, it remains very accurate (to within 1.5%) over the entire range of $\varepsilon$-values. In Section 7 (Fig. 6b), it is shown that the exact $\phi_{opt}$-values perfectly coincide with the $\phi^{1/2}$-line predicted by Eq. (33). The fact that Eq. (33) remains accurate in the $\varepsilon > 0.1$-range is surprising, because the $\phi_{opt}$-values in this range are also larger than 0.1, implicating that $Z$ can no longer be approximated by $Z_{tf}$, and also implicating that $m$ can no longer be approximated by $m \cong 4\phi$. The surprising accuracy of Eq. (33) can be understood by noting that it is the result of two different approximations who both have a nearly equal, but opposite effect on $C_{max}/t_{anal}$: considering $m \cong 4\phi$ instead of $m = 4\phi + 4\phi^2$ leads for large $\phi$ to an underestimation of $C_{max}$, while it has no effect upon $t_{anal}$; whereas approximating $Z$ by $Z_{tf}$ leads for large $\phi$ to an underestimation of $t_{anal}$, but has no effect upon $C_{max}$.

Considering Eq. (5b), and considering that the thin-film approximation (i.e., $Z = Z_{tf}$) can be written as $C'_s = k'.\phi^2/3.\varepsilon$ (cf. Eq. (5d)), Eq. (33) becomes:

$$\phi = \phi_{opt} \Leftrightarrow \frac{C'_m + C'_s}{C'_s} = \frac{C_m + C_s}{C_s} = 2, \text{ or:}$$

$$C_s = C_m \tag{34}$$

Eq. (34) shows that, for all $d$ and $k'$, the $C_{max}/t_{anal}$-ratio reaches its maximum when the stationary phase mass transfer resistance exactly makes up 50% of the total mass transfer resistance. This result is similar, but not identical, to a numerical result obtained by Tock et al. [13] for the maximisation of the mass loadability under the constraint of a maximally allowable analysis time (see also Section 6.2).

### 4.6. Simultaneously optimising $\phi$ and $d$ ($k'$ is a freely selectable constant)

The simultaneous optimisation of $\phi$ and $d$ is a trivial problem, because the equations for $\partial\Gamma/\partial\theta = 0$ and $\partial\Gamma/\partial\phi = 0$ are uncoupled. This implies that Eqs. (31)–(34) are valid for each column diameter, and hence also for $d = d_{opt}$.

### 4.7. Simultaneously optimising $\phi$ and $k'$ ($d$ is a freely selectable constant)

The simultaneous optimisation of $\phi$ and $k'$ requires the simultaneous solution of Eqs. (28) and (31). Again, an analytical solution does not exist because of the presence of a logarithm (via $Z$) in Eq. (31). However, as Eq. (33) very accurately approximates Eq. (31), it is obvious that the $Z = Z_{tf}$- and $m = 4\phi$-approximation can also be used to establish an approximate analytical expression for the present problem. Noting that $k'.\partial C'_s/\partial k' = C'_s$, and introducing the approximate $\phi = \phi_{opt}$-condition as $C'_s \cong C'_m$ (cf. Eq. 34), the optimisation of $\Gamma$ with respect to $k'$ for $\phi = \phi_{opt}$ can be approximated as:

$$2[(1 + k')^2 + \theta k'^2] = [-(1 + k')^3 + \theta(1 + k')k'^2] \cdot \left[\frac{k'}{C'_m} \cdot \frac{\partial C'_m}{\partial k'} + 1\right] \tag{35}$$

Replacing $C'_m$ by Eq. (5b) shows that Eq. (35) is of 5th-order in $k'$ and can hence only be solved with a root-finding numerical routine [25]. It should be noted that Eq. (35), which is only an approximate expression, no longer depends upon $\varepsilon$. This however does not affect its validity: it has been found that the $k'_{opt}$-values predicted by Eq. (35) typically deviate by no more than 2.5% from the values obtained by numerically solving the exact Eqs. (28) and (31). It has also been found that the $k'_{opt}$-values for the $C_{max}/t_{anal}$-optimisation reach their $\theta = \infty$-limit from about $\theta = 500$ on (see e.g., Fig. 9). Putting $\theta = \infty$ in Eq. (35), a 3rd order equation in $k'$ is obtained:

$$1 - k' - 23k'^2 - 33k'^3 = 0 \tag{36}$$

According to the Appendix, Eq. (36) can be solved to yield $k'_{opt} \cong 0.17$ (Eq. (A.6) with $n = 0$).

### 4.8. Simultaneously optimising $\phi$, $d$ and $k'$

Putting $\theta = \theta_{opt} = 2(1 + k')^2/k'^2$, and replacing $C'_m$ with Eq. (5b), Eq. (35) becomes:

$$5+23k'+12k'^2-33k'^3=0 \tag{37}$$

This is a 3rd order equation in $k'$, whose real positive root is given by $k'_{opt}=1.27$ (via Eq. (A.5)). Although Eq. (37) is only an approximate expression (because it is based upon Eq. (35)), it is shown in Section 7 that it remains an excellent approximation over the entire $\varepsilon$-range. Introducing the $k'_{opt}=1.27$-result into Eq. (23), the fully optimised $d_{opt}$-value (i.e., $d^*_{opt}$) is obtained. This value differs from the $d^*_{opt}$-value for the analysis time minimisation problem (see Fig. 6d), because the corresponding $k'_{opt}$-values are different.

## 5. Simultaneous optimisation of $C_{max}$, the column diameter, and $t_{anal}$

When considering radial, on-column optical detection methods, the $S/N$-ratio is, apart from $C_{max}$, also proportional to the column diameter, because the latter is a direct measure for the optical path length. To represent the simultaneous optimisation of $C_{max}$, $d$ and $t_{anal}$, the ratio of $C_{max}d/t_{anal}$ is considered. Starting from Eq. (27), and using Eq. (6b) to write $d$ as a function of $\theta$, the corresponding $\Gamma$-function can be written as:

$$\Gamma=\frac{m}{k'(1+k')}\cdot\frac{-1-2k'+(\theta-1)k'^2}{(C'_m+C'_s)\theta^{3/2}} \tag{38}$$

### *5.1. Optimising the column diameter d ($\phi$ and k′ are freely selectable constants)*

Maximising the $\Gamma$-function given in Eq. (38) with respect to $\theta$ yields:

$$\frac{\partial\Gamma}{\partial\theta}=0\Leftrightarrow\theta\,\frac{k'^2}{(1+k')^2}=3\Rightarrow\theta_{opt}=3\cdot\frac{(1+k')^2}{k'^2} \tag{39}$$

Eq. (39) is similar to Eq. (12), but the numerical constant now equals three instead of two. As a consequence, the factor 128 in Eq. (14) becomes a factor 192:

$$d_{opt}=\sqrt{\frac{192\mu ND_m}{\Delta P}} \tag{40}$$

Comparing Eq. (40) with Eq. (14) shows that, for a given value of $k'$, the $d_{opt}$-value for the $C_{max}d/t_{anal}$-optimisation is exactly $\sqrt{3/2}$ times larger than the $d_{opt}$-value for the $t_{anal}$- or the $C_{max}/t_{anal}$-optimisation. This result also has its impact on the optimal mobile phase velocity ($u'_{opt}$). Starting from Eq. (3) and replacing $d$ by its optimal value given in Eq. (40), the following expression for $u'_{opt}$ is obtained:

$$\Delta P=\frac{32\mu u'_{opt}N\text{HETP}}{\dfrac{192\mu ND_m}{\Delta P}}\Leftrightarrow u'_{opt}\text{HETP}=6D_m \tag{41}$$

Replacing HETP by its relation to the mobile phase velocity, Eq. (41) yields:

$$u'_{opt}\cdot\left(\frac{2D_m}{u'_{opt}}+2Cu'_{opt}\right)=6D_m \quad \text{or:}$$

$$u'_{opt}=\sqrt{\frac{2D_m}{C}} \tag{42}$$

Eq. (42) shows that when a maximal $C_{max}d/t_{anal}$-value is pursued, the column should no longer be operated at the minimum of the (HETP,$u$)-curve, i.e. at $u=u_{opt}=(D_m/C)^{1/2}$, but at a velocity which is exactly $\sqrt{2}$ times larger.

### *5.2. Optimising the film thickness ratio $\phi$ and the column retention factor k′*

It can easily be verified that the $\Gamma$-function in Eq. (38) has the same $\phi$-dependency as the $\Gamma$-function in Section 4. This implies that the $\phi_{opt}$-value for the $C_{max}d/t_{anal}$-optimisation is also given by Eqs. (31–34). The simultaneous optimisation of $d$ and $\phi$ is again trivial, because the equations for $\partial\Gamma/\partial\theta=0$ and $\partial\Gamma/\partial\phi=0$ remain uncoupled.

The $\Gamma$-function in Eq. (38) also has the same $k'$-dependency as the $\Gamma$-function in Section 4. The $k'_{opt}$-values for the $C_{max}d/t_{anal}$-optimisation are hence also given by Eq. (28), and the solution for large $\theta$ given by Eq. (29) is also still valid. The approximate solution for the simultaneous optimisation of $\phi$ and $k'$ (Eq. (35)) also remains valid.

### *5.3. Simultaneously optimising d and k′ ($\phi$ is a freely selectable constant)*

The simultaneous optimisation of $d$ and $k'$ is slightly different from the corresponding case in Section 4. This is due to the appearance of a factor three instead of two in the expression for $\theta_{opt}$. Putting $\theta = \theta_{opt} = 3(1+k')^2/k'^2$ in Eq. (28) yields:

$$2 + (6 + F)k' - (6 + F)k'^2 - 22k'^3 = 0, \tag{43}$$

The real positive root of Eq. (43) is, depending on $F$, given by either Eqs. (A.5) or (A.6).

### 5.4. Simultaneously optimising $\phi$, $d$ and $k'$

Putting $\theta = \theta_{opt} = 3(1+k')^2/k'^2$, and replacing $C'_m$ by Eq. (5b), Eq. (35) becomes:

$$3 + 11k' - k'^2 - 33k'^3 = 0, \tag{44}$$

from which (via Eq. (A.5)):

$$k'_{opt} = 0.669 \tag{45}$$

This result is validated in Section 7 (Fig. 6a). Slight deviations occur when $\varepsilon > 0.1$. This is due to the fact that Eq. (45) is based upon Eq. (35), which is only an approximate (but very accurate) expression.

## 6. Simultaneous optimisation of the mass flow-rate and $t_{anal}$

It is also possible to optimise the ratio of the mass flow-rate ($\sim C_{max}ud^2$) to the analysis time. This is especially relevant for mass-flow sensitive detectors [26]. Similar to the derivation of Eq. (38), the optimisation of the ratio of $C_{max}.u.d^2/t_{anal}$ can be rewritten in terms of a dimensionless goal function $\Gamma$:

$$\Gamma = \frac{m}{k'(1+k')} \cdot \left( \frac{-(1+k')^2 + \theta k'^2}{(C'_m + C'_s)\theta} \right)^{3/2} \tag{46}$$

### 6.1. Optimising the column diameter $d$ ($\phi$ and $k'$ are freely selectable constants)

Differentiating $\Gamma$ with respect to $\theta$, it is found that:

$$\frac{\partial \Gamma}{\partial \theta} = 0 \Leftrightarrow \frac{-(1+k')^2 + \theta k'^2}{\theta^2} = 0 \tag{47}$$

Eq. (47) has two solutions. One, given by $\theta = (1+k')^2/k'^2$, corresponding to the minimum of $\Gamma$ (i.e., $\Gamma = 0$), and one, given by $\theta = \infty$ and corresponding to the maximum of $\Gamma$ ($\Gamma_{max}$):

$$\Gamma = \Gamma_{max} = \frac{m}{(1+k')} \cdot \frac{k'^2}{(C'_m + C'_s)^{3/2}} \Leftrightarrow \theta = \infty \tag{48}$$

The latter condition is however not practically useful because it leads to infinite analysis times. Now, plotting $\Gamma$ versus $\theta$ for a number of different conditions, it was found that $\Gamma$ always increases rapidly with $\theta$ when $\theta$ is small, but that the rate of increase gradually drops to zero when $\theta$ is larger than 50 to 100. This implies that a sufficiently large fraction of $\Gamma_{max}$ is already reached at relatively small values of $\theta$. Also considering that $t_{anal}$ increases dramatically when $\theta > 100$, an optimisation scheme is proposed which is based upon a sub-optimal $\theta$-value, i.e. a value at which $\Gamma$ reaches a given (large) fraction of its maximum ($\Gamma_{max}$). Investigating a large variety of different conditions, it was found that a value of $\Gamma/\Gamma_{max} = 2/3$ yields a good compromise between a large $C_{max}.u.d^2/t_{anal}$-value and a reasonable analysis time. Dividing Eq. (46) by Eq. (48), the following expression for the $\Gamma/\Gamma_{max} = 2/3$-condition is obtained:

$$\frac{\Gamma}{\Gamma_{max}} = \frac{2}{3} \Leftrightarrow \theta_{opt} = \frac{1}{1 - \left(\frac{2}{3}\right)^{2/3}} \cdot \frac{(1+k')^2}{k'^2} \cong 4.22 \cdot \frac{(1+k')^2}{k'^2} \tag{49}$$

Comparing the numerical constant in Eq. (49), with the numerical constants in Eqs. (12) and (39), a certain numerical order and logic (cf. Table 1) can be discerned when passing from the $C_{max}/t_{anal}$-optimisation (constant = 2), over the $C_{max}.d/t_{anal}$-optimisation (constant = 3), towards the $C_{max}.u.d^2/t_{anal}$-optimisation (constant ≅ 4).

### 6.2. Optimising the film thickness ratio $\phi$ ($d$ and $k'$ are freely selectable constants)

Optimising $\Gamma$ (Eq. 46) with respect to $\phi$ yields:

Table 1
Optimization rules for the different investigated criteria

| Criterion | $\theta_{opt}$ | $u_{opt}$ | $(C_s/C)_{opt}$ | $\phi_{opt}$ | $k'_{opt}$ [b] |
|---|---|---|---|---|---|
| $t_{anal}$ | $2\cdot\frac{(1+k')^2}{k'^2}$ | $\sqrt{\frac{D_m}{C}}$ | $C_s/C\rightarrow 0$ | $\phi\rightarrow 0$ | 2.69 |
| $C_{max}/t_{anal}$ | $2\cdot\frac{(1+k')^2}{k'^2}$ | $\sqrt{\frac{D_m}{C}}$ | 1/2 | $\sqrt{3\cdot\frac{(1+6k'+11k'^2)}{192.k'}\,\varepsilon}$ | 1.27 |
| $C_{max}.d/t_{anal}$ | $3\cdot\frac{(1+k')^2}{k'^2}$ | $\sqrt{2\cdot\frac{D_m}{C}}$ | 1/2 | $\sqrt{3\cdot\frac{(1+6k'+11k'^2)}{192.k'}\,\varepsilon}$ | 0.669 |
| $C_{max}.u.d^2/t_{anal}$ [a] | $4.22\cdot\frac{(1+k')^2}{k'^2}$ | $\sqrt{3.22\cdot\frac{D_m}{C}}$ | 1/3 | $\sqrt{\frac{3}{2}\cdot\frac{(1+6k'+11k'^2}{192.k'}\,\varepsilon}$ | 0.439 |

[a] The factor 4.22 in the $\theta_{opt}$-expression is the result of the arbitrary choice of $\Gamma/\Gamma_{max}=2/3$ (cf. Eq. (49)). Selecting a factor of four instead of 4.22 could be considered as well. In this case, the different factors in the $\theta_{opt}$-expressions would form a perfect geometric series. Taking $\theta_{opt}=4(1+k')^2/k'^2$, the corresponding $u_{opt}$-value would be given by $(3D_m/C)^{1/2}$.
[b] The represented $k'_{opt}$-values are for the $d=d_{opt}$- and $\phi=\phi_{opt}$-case.

$$\frac{\partial\Gamma}{\partial\phi}=0\Leftrightarrow\left[\frac{1+6k'+11k'^2}{192}+k'\,\frac{Z}{3\varepsilon}\right]\cdot\frac{3\varepsilon}{k'}\cdot(1+2\phi)=\frac{3}{2}\,\phi(1+\phi)\,\frac{dZ}{d\phi} \tag{50}$$

Eq. (50) only differs from Eq. (31) by the presence of a factor 3/2 on its right hand side. Just as for Eq. (31), a very accurate approximate solution for Eq. (50) can be established by considering the $Z=Z_{tf}$- and $m=4\phi$-approximation. In this case, Eq. (50) reduces to:

$$\frac{1}{192}\cdot(1+6k'+11k'^2)+k'\cdot\frac{\phi^2}{3.\varepsilon}=k'\cdot\frac{\phi^2}{\varepsilon} \tag{51}$$

From Eq. (51), the (approximated) optimal $\phi$-value can be directly obtained:

$$\phi_{opt}=\sqrt{\frac{3}{2}\cdot\frac{(1+6k'+11k'^2)}{192k'}\cdot\varepsilon} \tag{52}$$

The accuracy of Eq. (52) is better than 2% over the entire $\varepsilon$-range (see Fig. 6b). The reason for this excellent accuracy is identical to the reason for the excellent accuracy of Eq. (33). Comparing Eq. (52) with Eq. (33) shows that the $\phi_{opt}$-value for the $C_{max}ud^2/t_{anal}$-optimisation is exactly $\sqrt{2}$ times smaller than for the $C_{max}/t_{anal}$- or the $C_{max}d/t_{anal}$-optimisation. Similar to Eq. (32), Eq. (51) can also be rearranged in terms of $C'_m$ and $C'_s$:

$$\phi=\phi_{opt}\Leftrightarrow\frac{C'_m+C'_s}{C'_s}=3\quad\text{or: }C_s=\frac{1}{2}\cdot C_m \tag{53}$$

Eq. (53) shows that when a maximal $C_{max}ud^2/t_{anal}$-ratio is pursued, $\phi$ should be selected such that $C_s/C=1/3$, instead of according to the $C_s/C=1/2$-condition for the $C_{max}/t_{anal}$- and the $C_{max}.d/t_{anal}$-maximisation. Just as Eq. (34), Eq. (53) is only exact when $\phi_{opt}$ is small enough to justify the thin-film approximation (i.e., when $\varepsilon\leq 0.1$). When $\varepsilon>0.1$, the optimal $C_s/C$-value is slightly larger than 1/3 (see Fig. 6d). The $C_s/C=1/3$-result corresponds exactly to the optimisation rule numerically obtained by Tock et al. [13]. The fact that an identical optimisation rule is obtained, despite of the fundamental difference between the presently considered optimisation problem ($t_{anal}$ is free) and the problem considered by Tock et al. ($t_{anal}$ is imposed), is a clear indication for the universal character of this rule. The link between both problems will be further investigated in a following study.

### 6.3. *Optimising the column retention factor k′ (d and $\phi$ are freely selectable constants)*

Maximising $\Gamma$ with respect to $k'$ yields a 5th order equation which has to be solved with a numerical root-finding routine, and by accounting for Eq. (19).

### 6.4. Optimising the column retention factor $k'$ when $d \gg d_{opt}$

An analytically solvable expression for the maximisation of $\Gamma$ with respect to $k'$ only exists for the $\theta=\infty$-limit. In this case, a 3rd order equation in $k'$ is obtained:

$$4+(6+F)k'-(28+F)k'^2-44k'^3=0 \qquad (54)$$

The feasible root of Eq. (54) is given by Eq. (A.6), with, depending upon the value of $F$, either $n=0$ or $n=1$. Considering typical values of $\varepsilon=0.1$ and $\phi=0.1$, this yields $k'_{\mathrm{opt}}=0.44$.

### 6.5. Simultaneously optimising $d$ and $k'$ ($\phi$ is a freely selectable constant)

Replacing $\theta$ by $\theta_{\mathrm{opt}}=4.22(1+k')^2/k'^2$ in Eq. (46) and optimising the resulting expression with respect to $k'$, the following 5th order equation is obtained:

$$[1+k'+(2\theta-1)k'^2+(\theta-1)k'^3](C'_{\mathrm{m}}+C'_{\mathrm{s}}) = \frac{3}{2}(k'+k'^2)[\theta k'^2-(1+k')^2]\frac{\partial(C'_{\mathrm{m}}+C'_{\mathrm{s}})}{\partial k'} \qquad (55)$$

### 6.6. Simultaneously optimising $\phi$ and $k'$ ($d$ is a freely selectable constant)

From the excellent accuracy of Eq. (53), it follows that the simultaneous optimisation of $\phi$ and $k'$ can be very accurately represented by combining Eqs. (53) and (55). Dividing Eq. (55) by $C'_{\mathrm{s}}$, putting $C'_{\mathrm{s}}=1/2C'_{\mathrm{m}}$ (Eq. 53), and noting that $k'\partial C'_{\mathrm{s}}/\partial k'=C'_{\mathrm{s}}$, yields:

$$2[1+k'+(2\theta-1)k'^2+(\theta-1)k'^3]=(k'+k'^2)[\theta k'^2-(1+k')^2]\cdot\left[\frac{k'}{C'_{\mathrm{s}}}\frac{\partial C'_{\mathrm{m}}}{\partial k'}+1\right] \qquad (56)$$

This equation is of 4th order in $k'$, and should hence preferably be solved numerically.

### 6.7. Simultaneously optimising $\phi$, $d$ and $k'$

Putting $\theta=\theta_{\mathrm{opt}}=4.22(1+k')^2/k'^2$, Eq. (56) remains of 4th order. Numerically solving it, this yields $k'_{\mathrm{opt}}=0.439$ for all $\varepsilon\leq0.1$. When $\varepsilon>0.1$, $k'_{\mathrm{opt}}$ becomes slightly larger (cf. Fig. 6a).

## 7. Discussion of the optimisation rules

### 7.1. Variation of $C_{max}/t_{anal}$ with $d$, $\phi$, and $k'$

Fig. 3a shows the gain in $C_{\mathrm{max}}/t_{\mathrm{anal}}$ under optimised $d$-, $\phi$-, and $k'$-conditions. To obtain a plot containing all combinations of $d$, $\alpha_{\mathrm{s}}$, $R_{\mathrm{s}}$, $D_{\mathrm{m}}$, $\mu$ and $\Delta P$, the $C_{\mathrm{max}}/t_{\mathrm{anal}}$-values are normalised by dividing them by the largest possible $C_{\mathrm{max}}/t_{\mathrm{anal}}$-value, i.e., the value for $k'=k'_{\mathrm{opt}}$, $\phi=\phi_{\mathrm{opt}}$ and $\theta=\theta_{\mathrm{opt}}=6.4$. The data in Fig. 3a are for $\varepsilon=0.5$ ($\varepsilon=D_{\mathrm{s}}/D_{\mathrm{m}}$), but it has been verified that fully similar curves are obtained for all relevant $\varepsilon$-values ($10^{-3}\leq\varepsilon\leq1$). Fig. 3b shows the curves of Fig. 3a, after division by the values of curve (d). After this transformation, curve (d) is reduced to a horizontal line with value unity (Fig. 3b) and the other curves directly show the decreased performance caused by the use of a non-fully optimised set of $\phi$- and $k'$-values. The impact is obviously most significant when the column is operated near its efficiency limit (i.e., when $\theta\rightarrow1$). On the other end of the $\theta$-domain, all performance curves tend to a limiting value from about $\theta=100$ on.

Apart from the strong variation in the $\theta$-domain, the $C_{\mathrm{max}}/t_{\mathrm{anal}}$-values also vary strongly in the $\phi$-domain (Fig. 4). This means that the selection of an appropriate film thickness is as important as the selection of an appropriate column diameter. Plots of the variation of $C_{\mathrm{max}}d/t_{\mathrm{anal}}$ and $C_{\mathrm{max}}ud^2/t_{\mathrm{anal}}$ with $\phi$ were found to be completely similar to Fig. 4.

Although Figs. 3 and 4 clearly demonstrate the importance of optimised $\phi$- and $d$-values, it should be noted that $\phi$ and $d$ can generally not be freely selected. This is due to practical limitations, such as the lack of adequate coating techniques [4–6], and such as the obligation to use supra-optimal column diameters to cope with the insufficient sensitivity of LC detectors [1,7,8]. With $\phi$ and $d$ constrained, the retention factor $k'$ becomes the most important design variable. The steep curve slopes in Fig. 5 clearly show the large gain which can be obtained by selecting $k'$ close to the $k'_{\mathrm{opt}}$-value given by Eq. (17). Fig. 5 shows that for a $\theta=281$ column, the $C_{\mathrm{max}}/t_{\mathrm{anal}}$-ratio can be increased by a factor of 8.4 as compared to a separation at $k'=3$. As the shift from $k'=3$ to $k'=k'_{\mathrm{opt}}$ also brings about a small (and hence easily tolerable) increase of $t_{\mathrm{anal}}$ (factor of

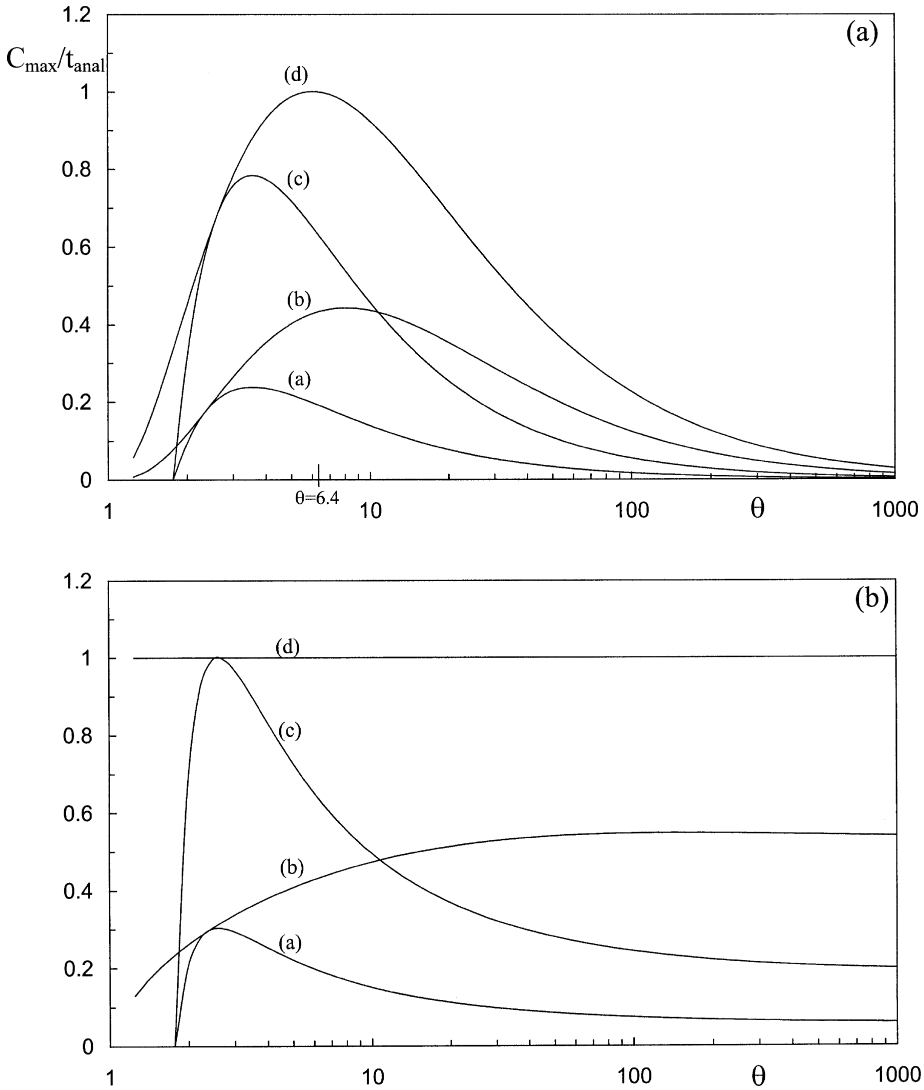


Fig. 3. (a) Normalised $C_{max}/t_{anal}$-values versus $\theta$ for $\varepsilon=0.5$ and for four different cases: (a) $k'=3$ and $\phi=0.1$, (b) $k'=k'_{opt}$ and $\phi=0.1$, (c) $k'=3$ and $\phi=\phi_{opt}$ and (d) $k'=k'_{opt}$ and $\phi=\phi_{opt}$. (b) Representation of the data of (a) as $[C_{max}/t_{anal}(\theta, k', \phi)]/[C_{max}/t_{anal}(\theta, k'_{opt}, \phi_{opt})]$ versus $\theta$.

1.35), the increase of $C_{max}/t_{anal}$ with a factor of 8.4 in fact corresponds to an even larger increase of $C_{max}$ (factor of 11.3). Considering that it are especially detection problems which form the bottleneck of OT-LC, this is an advantageous feature. It was also found that the slope of the curves becomes steeper with increasing $\theta$. The advantage of working around $k'_{opt}$ is hence most important when $d \gg d_{opt}$, a condition which holds for most separations in 5 μm-columns. Plots of the variation of $C_{max}.d/t_{anal}$ and $C_{max}.u.d^2/t_{anal}$ with $k'$ were found to be completely similar: the curve slopes are nearly equally steep and the optima also lie in the range of $k'=0.3$ to 0.5.

### 7.2. Influence of $D_s/D_m$

Fig. 6 has been established to obtain a better

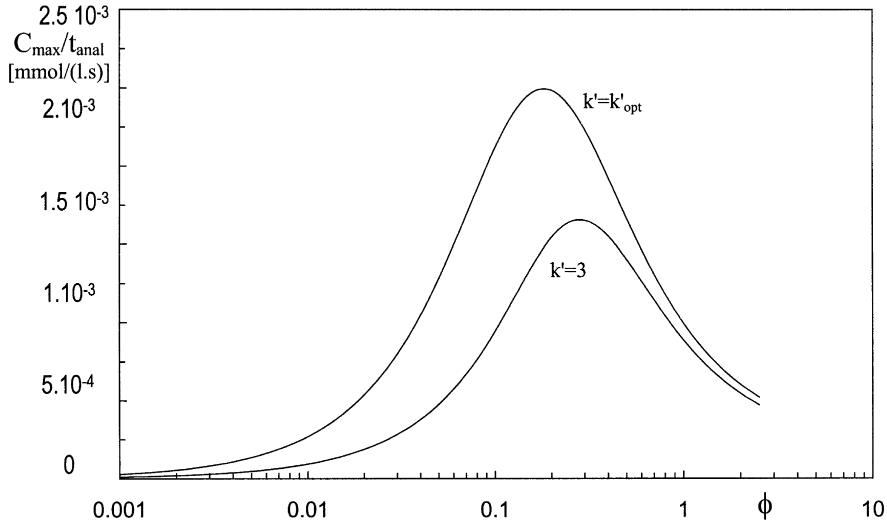


Fig. 4. $C_{max}/t_{anal}$ versus $\phi$ ($d=d_{opt}$, $\varepsilon=0.5$).

insight in the difference between the pure minimal $t_{anal}$-criterion and the relative criteria $C_{max}/t_{anal}$, $C_{max}d/t_{anal}$ and $C_{max}ud^2/t_{anal}$. All presented data correspond to the fully optimised case: for each considered $\varepsilon$-value, the corresponding $k'=k'_{opt}$, $\phi=\phi_{opt}$ and $\theta=\theta_{opt}$-values were used. Fully similar graphs are however obtained when $k'$, $\theta$ and/or $\phi$ are kept at a non-optimal value. It should be noted that all case (a)-curves have been obtained by selecting $\phi$ such that $C_s/C=0.01$ for each $\varepsilon$-value (cf. Fig. 6d). Although it does not correspond to the mathematically exact condition (i.e., $t_{anal}$ is minimal when $C'_s\rightarrow 0$), this condition at least yields $\phi$- and $C_{max}$-values which are not insignificantly small, while the corresponding $t_{anal}$-values are only slightly larger (about 1%) than the exact minimal analysis times.

Fig. 6a clearly shows that $k'_{opt}$ shifts to ever

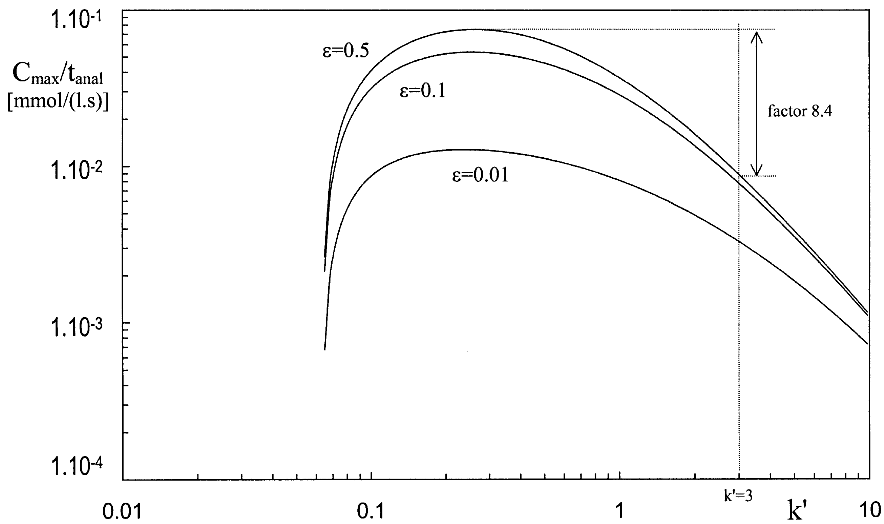


Fig. 5. $C_{max}/t_{anal}$ versus $k'$ for a given set of non-optimized, but typical state-of-the-art column parameters ($d=5$ μm and $\phi=0.1$) and for $\alpha_s=1.03$ ($\theta=281.2$).

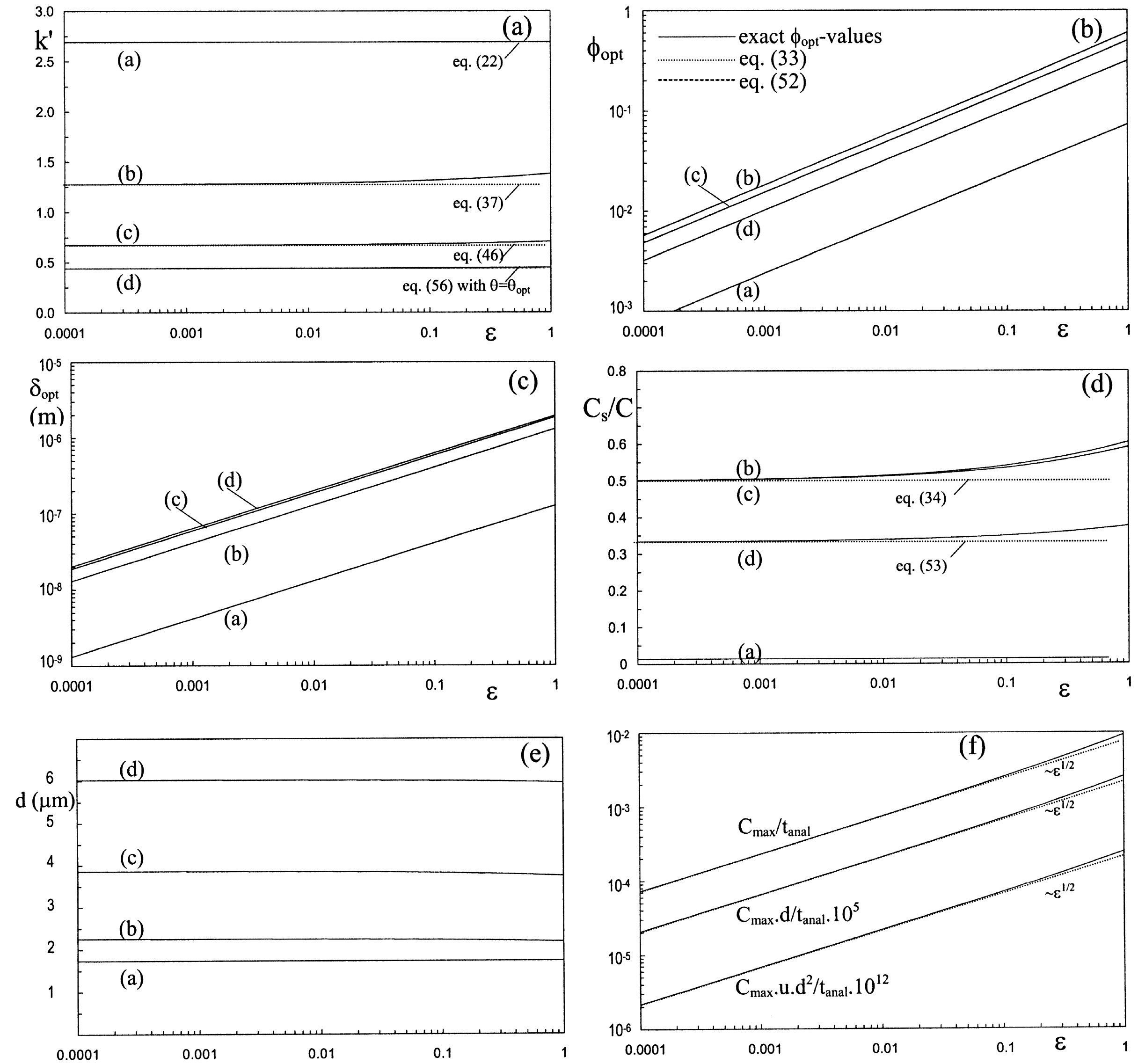


Fig. 6. Optimisation characteristics for the minimization of $t_{anal}$ (case a), the maximisation of $C_{max}/t_{anal}$ (case b), the maximization of $C_{max}d/t_{anal}$ (case c) and the maximisation of $C_{max}ud^2/t_{anal}$ (case d): (a) $k'_{opt}$ versus $\varepsilon$ ($d=d_{opt}$ and $\phi=\phi_{opt}$), (b) corresponding $\phi_{opt}$-values, (c) corresponding $\delta_{opt}$-values ($\delta_{opt}=d_{opt}.\phi_{opt}$), (d) corresponding $C_s/C$-values, (e) corresponding $d_{opt}$-values, (f) variation of $C_{max}/t_{anal}$, $C_{max}d/t_{anal}$ and $C_{max}ud^2/t_{anal}$ with $\varepsilon$ (dashed lines represent $\varepsilon^{1/2}$-dependency).

smaller values when passing from case (a) to case (d). As can be noted, the exact $k'_{opt}$-values can be very well approximated by the analytical expressions of Sections 3–6. Fig. 6b and c clearly show that $\phi_{opt}$ and $\delta_{opt}$ exactly vary according to $\varepsilon^{1/2}$ for all three considered criteria. This confirms the accuracy of the approximated analytical results given by Eqs. (33) and (52). Fig. 6d clearly shows that $C_{max}ud^2/t_{anal}$ is optimal around $C_s/C=1/3$, while the two other relative performance criteria reach their optimum around $C_s/C=1/2$. Whereas the presented $C_s/C$-curves are for $k'=k'_{opt}$, it has been verified that fully similar curves are obtained for other, non-optimal $d$- and $k'$-values. The slight increase of the optimal

$C_s/C$-values when $\varepsilon > 0.1$ can be explained by the fact that the $\phi_{opt}$-values in this range are also larger than 0.1. As a consequence, the quadratic term in $m$ ($m = 4\phi + 4\phi^2$) starts to dominate. Apparently, this positive effect on the detectability more than outweighs the corresponding increase of $t_{anal}$. Hence, the net result of the thick-film effects is that they shift the optimum conditions towards a larger stationary phase mass transfer contribution. The consistent increase of $d_{opt}$ (Fig. 6e) when passing from case (a) to case (d) is in agreement with the increasing importance which is attributed to the amount of mass which passes the detector per unit of time in the corresponding optimisation criteria. It is however surprising that the different $d_{opt}$-values differ by no more than a factor of three. Fig. 6f shows that the fully optimised performance ratio's vary according to $\varepsilon^{1/2}$ when $\varepsilon \leq 0.1$. When $\varepsilon > 0.1$, the $\varepsilon$-dependency is even slightly stronger. Similar to Fig. 6d, this reflects the fact that the increase of $t_{anal}$ caused by the thick-film diffusion effect is less important than the increase of $C_{max}$ originating from the domination of the second order term in $m = 4\phi + 4\phi^2$. Fig. 6f hence provides a clear quantitative argument for the development of coating strategies [6,10,11] yielding large stationary phase diffusion rates.

### *7.3. Absolute $C_{max}$- and $t_{anal}$-values under optimized conditions*

As the performance criteria identified in Sections 4–6 are only relative measures, it has to be verified whether they do not reach their optimum at unallowably large $t_{anal}$- or at insignificantly small $C_{max}$-values. In Figs. 7 and 8, the absolute $t_{anal}$- and $C_{max}$-values under fully optimised $C_{max}/t_{anal}$-, $C_{max}d/t_{anal}$- and $C_{max}ud^2/t_{anal}$-conditions are compared to the case in which $\phi$ and $k'$ are optimised with the single aim of minimising $t_{anal}$ (curve a) and to the case in which $\phi$ and $k'$ are optimised with the single aim of maximising $C_{max}$ (curve e). For the latter case, a restriction on the analysis time had to be imposed in order to avoid infinite analysis time results. Curve (e) therefore refers to the case in which, for each value of $\theta$, $C_{max}$ is maximised while keeping $t_{anal}$ at a value which is exactly ten times larger than the minimal $t_{anal}$ for that given $\theta$-value. In order to unify all possible combinations of $d$, $\alpha_s$, $R_s$, $D_{mol}$ and $\Delta P_{max}$, the data in Fig. 7a have been normalised with respect to the absolute minimal analysis time, i.e., the time obtained for $\theta = \theta_{opt}$ in case (a). In Fig. 7b, the $t_{anal}$-data of Fig. 7a are transformed by dividing them by the values of curve (a). According to this procedure, curve (a) and (e) become straight, horizontal lines, and the other curves directly show the relative increase in $t_{anal}$ when adopting one of the relative performance criteria, In a similar way, the $C_{max}$-curves of Fig. 8a have been transformed into the relative curves of Fig. 8b. It should also be noted that, similar to Fig. 6, the $C_{max}$-values for curve (a) have been obtained by considering $C_s/C = 0.01$ instead of the mathematically exact condition of $C_s/C \rightarrow 0$. The perfect coincidence of curves (b) and (c) in both Figs. 7 and 8 can be explained from the discussion in Section 5.2 (see also Fig. 9).

Considering a given $\theta$-value, Fig. 7b clearly shows that the $C_{max}/t_{anal}$-optimisation increases the analysis time with about a factor of two to five as compared to the minimal analysis time for that given $\theta$-value. This increase in $t_{anal}$ is however rewarded by a large increase (a factor of about 15 to 30) in $C_{max}$. Fig. 8b also clearly shows that curves (b) and (c) are in fact already very close to curve (e), representing the $C_{max}$-values which can maximally be obtained when $t_{anal}$ is allowed to be ten times as large as the minimal analysis time for that given $\theta$-value. Considering the $t_{anal}$-values under optimised $C_{max}.u.d^2/t_{anal}$-conditions (d-curves), it is surprising to note that they are much smaller than for the optimal $C_{max}/t_{anal}$-conditions. The corresponding gain in $C_{max}$ is however also smaller (gain factor maximally of the order of ten, see curve d – Fig. 8b).

In general, it can be concluded from Figs. 7 and 8 that all three considered optimisation criteria lead to 'reasonable' absolute $t_{anal}$ and $C_{max}$-values, i.e. the corresponding optimisation rules yield a substantial increase in detectability without leading to impractically large analysis times. It should be noted that, whereas Figs. 7 and 8 are for $\varepsilon = 0.1$, fully similar curve sets are obtained for all other practical $\varepsilon$-values. The above conclusions hence hold for all values of $\varepsilon$. It has also been verified that a similar conclusion can be drawn when $C_{max}d$ or $C_{max}ud^2$ are considered instead of $C_{max}$ in Fig. 8.

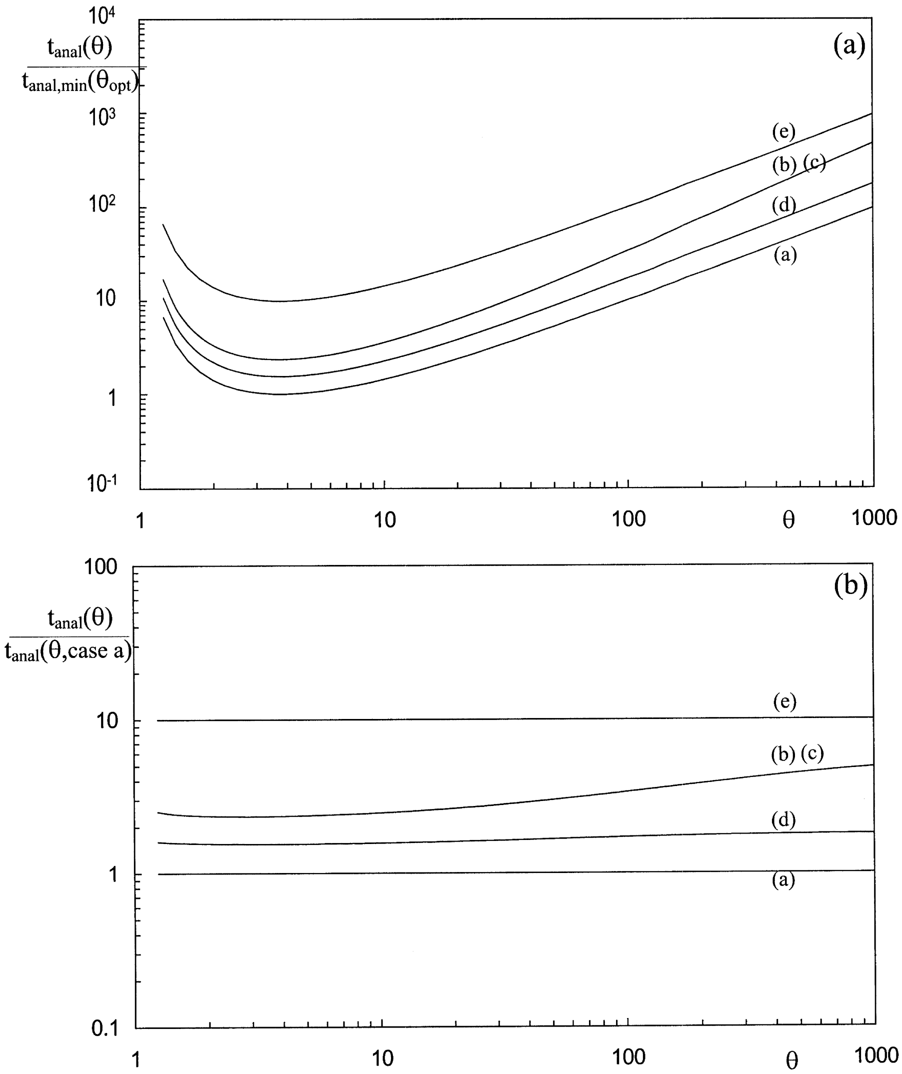


Fig. 7. (a) Variation of $t_{anal}$ with $\theta$ ($\varepsilon = 0.1$) under optimized $t_{anal}$- (curve a), $C_{max}/t_{anal}$- (curve b), $C_{max}d/t_{anal}$- (curve c) and $C_{max}ud^2/t_{anal}$-conditions (curve d). Curve (e) is obtained by maximizing $C_{max}$ under the restriction of $t_{anal}(\theta) = 10t_{anal,min}(\theta)$. (b) Normalised representation of the $t_{anal}$-values given in (a).

Fig. 9 shows how $k'$ has to be varied with $\theta$ in order to obtain the fully optimised curves presented in Figs. 7 and 8. The fact that curves (b) and (c) coincide is again in agreement with the discussion held in Section 5.2. As can be noted, all four optimisation criteria lead to extremely large $k'_{opt}$-values when $\theta < \theta_{opt}$, and to very small $k'_{opt}$-values ($k'_{opt} < 1$) when $\theta \gg \theta_{opt}$. It can also be noted that all $k'_{opt}$-curves reach a limiting value from about $\theta = 100$ to 500 on. Fig. 9 also shows that the $k'_{opt}$-curves for $\varepsilon = 0.5$, $\varepsilon = 0.1$ and $\varepsilon = 0.001$ nearly perfectly coincide. It can hence be concluded that the $k'_{opt}$-values only depend very weakly upon $\varepsilon$. Fig. 9 can hence be used to directly read out the optimal $k'$-value ($\phi = \phi_{opt}$-case) for each given value of $\theta$ and $\varepsilon$.

## 8. Conclusions

An analytical solution for Scott's analysis time

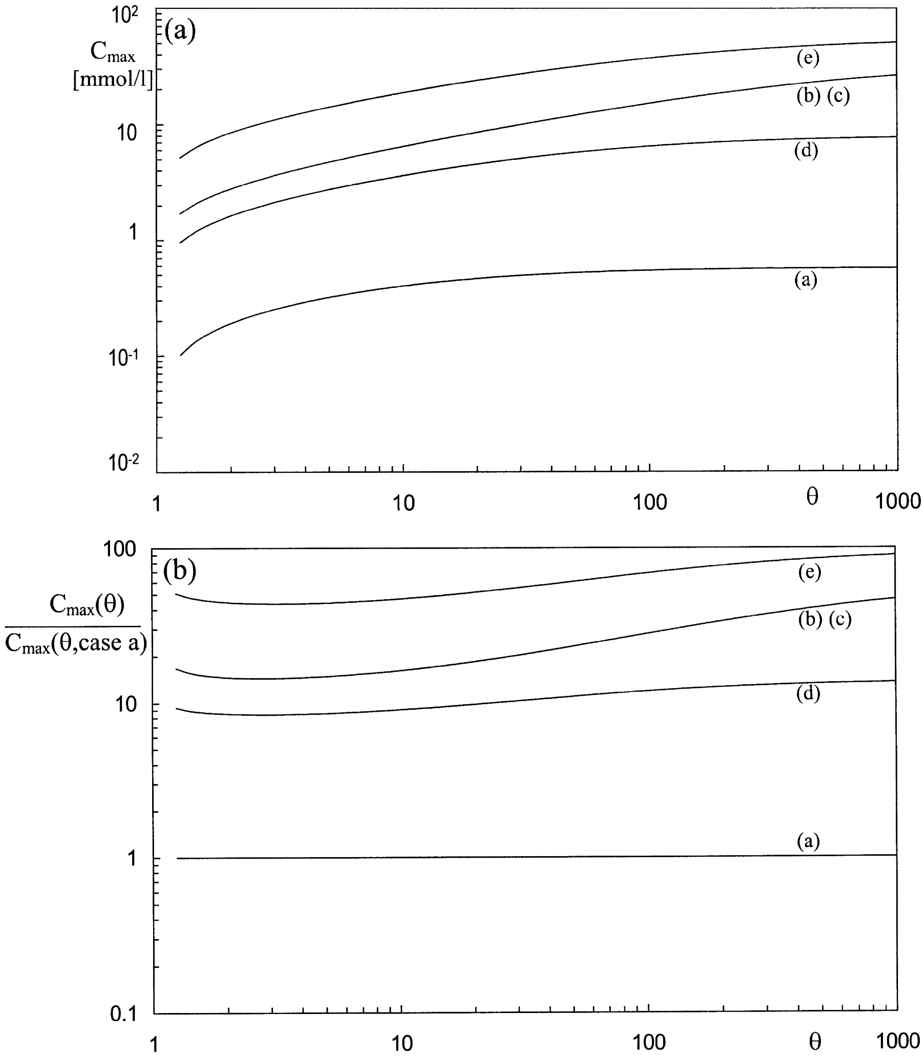


Fig. 8. (a) Variation of $C_{max}$ with $\theta$ ($\varepsilon = 0.1$) under optimised $t_{anal}$- (curve a), $C_{max}/t_{anal}$- (curve b), $C_{max}d/t_{anal}$- (curve c) and $C_{max}ud^2/t_{anal}$-conditions (curve d). Curve (e) is obtained by maximising $C_{max}$ under the restriction of $t_{anal}(\theta) = 10t_{anal,min}(\theta)$. (b) Normalised representation of the $C_{max}$-values given in (a).

minimisation problem ($d = d_{opt}$ and $\phi \ll 1$) can be established ($k'_{opt} = 2.69$). The mathematical analysis can also be extended to columns with a thick stationary phase film and/or with a non-optimal diameter. The introduction of the dimensionless $\theta$-number considerably simplifies the design rules because it groups the influence of $d$, $\alpha_s$, $R_s$, $D_{mol}$ and $\Delta P_{max}$ into a single variable. For thin-film columns for example, the established equations show that $k'_{opt}$ shifts from $k'_{opt} = 2.69$ for $d = d_{opt}$ when $k'_{opt} = 0.91$ when $d \gg d_{opt}$. For the $d = d_{opt}$-case, the equations allow to directly calculate how $k'_{opt}$ increases from $k'_{opt} = 2.69$ for $\phi \ll 1$ to $k'_{opt} > 10$ for $\phi > 0.1$.

The mathematical analysis can also be extended to a number of relative performance criteria ($C_{max}/t_{anal}$, $C_{max}d/t_{anal}$, $C_{max}ud^2/t_{anal}$), in which the need for concentrated, easily detectable peaks is balanced against the requirement of a short analysis time. As these criteria give rise to directly usable (cf. Table 1) and 'reasonable' (cf. Figs. 7 and 8) design rules, they

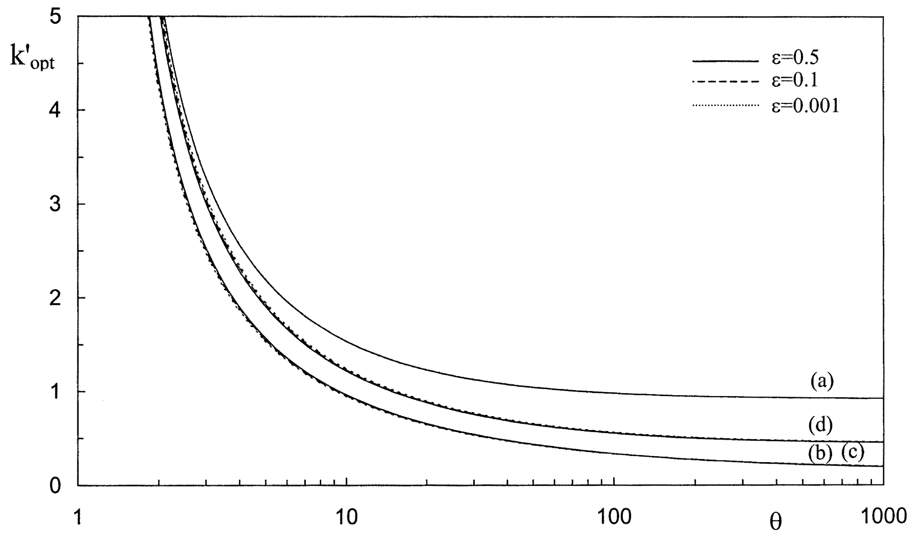


Fig. 9. $k'_{opt}$ versus $\theta$ under fully optimised $t_{anal}$- (curve a), $C_{max}/t_{anal}$- (curve b), $C_{max}d/t_{anal}$- (curve c) and $C_{max}ud^2/t_{anal}$-conditions (curve d).

are excellently suited to be used as easy identifiable landmarks in the complex ($R_s$, $C_{max}$, $t_{anal}$)-space. Considering for example the $\phi$-domain curves in Fig. 2, knowing whether a given system is situated on the left, *resp.* right hand side of the optimum learns whether an increase of the film thickness leads to an increase of the analysis time which is smaller, *resp.* larger than the corresponding increase in $C_{max}$. Similar design information can be obtained in the $k'$- and the $d$-domain. Combining these pieces of information with the true economic value of $C_{max}$ and $t_{anal}$ then allows to estimate whether there is room to substantially improve a given OT-LC system or not, and how this should best occur. Another insight provided by the $t_{anal}$-based relative performance criteria is that, for a column with for example $\theta=100$, a tripling of the analysis time might lead to a 20-fold increase of the peak concentration (cf. Figs. 7 and 8). This might appear attractive, but it also points at the weakness of OT-LC, because it also implies that any attempt to increase the detectability by more than a factor of 20 begins to cost more and more in terms of the analysis time. Again, what this 'cost' means in real economical terms, and what additional cost beyond this optimal point can be afforded, is to be decided for each application individually.

The present analysis also clearly demonstrated that the concentration detectability in OT-LC columns can be strongly increased by designing columns in which the $C_s$-term makes up 33 to 50% of the total $C$-term, thereby confirming and extending a previous numerical analysis presented by Tock et al. [13]. The problem of the small column diameters and the correspondingly small mass loadability however remains, and is clearly inherent to the nature of OT-LC. This is for example reflected by the fact that the optimal column diameter for the $C_{max}ud^2/t_{anal}$-optimisation is only three times larger than the optimal diameter for the pure $t_{anal}$-minimisation (see Fig. 6a). This observation once more provides an additional argument for the need for novel, more sensitive detection methods in OT–LC.

## 9. Symbols

| | |
|---|---|
| $A$ | non-optimisable part of $C_{max}$-expression, see Eq. (10), [mol/m$^3$] |
| $C$ | mass transfer contribution to HETP, see Eq. (2), [s] |
| $C'$ | dimensionless mass transfer contribution to HETP, see Eq. (5), [/] |
| $C_{max}$ | peak concentration of given component in chromatogram, [mol/m$^3$] |

| | |
|---|---|
| $d$ | column diameter, [m] |
| $d^*_{opt}$ | optimal column diameter under optimal $k'$-conditions, see Eq. (23), [m] |
| $D$ | molecular diffusion coefficient, [$m^2/s$] |
| $F$ | dimensionless number, proportional to the stationary phase mass transfer resistance, see Eq. (18) |
| HETP | height of equivalent theoretical plate, [m] |
| $k'$ | retention factor, [/] |
| $K$ | distribution coefficient, [/] |
| $m$ | phase volume ratio, [/] |
| $m_{30}$ | reduced load, $m_{30}=2$ [13] |
| MW | molecular weight of sample component, MW=200 g/mol [13] |
| $N$ | theoretical plate number, [/] |
| $R$ | discriminant, see Eq. (A.4) |
| $R_s$ | resolution factor, [/] |
| $t_{anal}$ | analysis time, [s] |
| $u$ | mean mobile phase velocity, [m/s] |
| $u'_{opt}$ | optimal mobile phase velocity for $C_{max}.d/t_{anal}$, see Eq. (42), [m/s] |
| $Z$ | dimensionless parameter expressing the radial stationary phase diffusion, see Eq. (5). |

*Greek symbols*

| | |
|---|---|
| $\alpha_s$ | separation factor, [/] |
| $\delta$ | stationary film thickness, [m] |
| $\Delta P$ | pressure drop, [bar] |
| $\varepsilon$ | $D_s/D_m$-ratio, [/] |
| $\phi$ | phase thickness ratio ($\phi=\delta/d$), [/] |
| $\Gamma$ | optimizable goal function, see Eqs. (9b), (27), (38) and (46), [/] |
| $\mu$ | dynamic viscosity, [kg/(m.s)] |
| $\theta$ | dimensionless number relating the column diameter to $\Delta P$, see Eq. (6b), [/] |
| $\rho_{sf}$ | stationary phase density, $\rho_{sf}=10^3$ kg/m$^3$ [13] |

*Subscripts*

| | |
|---|---|
| m | mobile phase |
| min | minimum |
| opt | optimum |
| s | stationary phase |
| tf | thin-film |

## Appendix

When considering a given 3rd order equation,

$$a_0 + a_a x + a_2 x^2 + x^3 = 0, \tag{A.1}$$

its real roots can be obtained according to the following procedure [25]. First, the variables $p$ and $q$ have to be calculated according to:

$$p = \frac{1}{9}\cdot(3a_1 - a_2^2) \tag{A.2}$$

$$q = \frac{1}{54}\cdot(27a_0 - 9a_1a_2 + 2a_2^2) \tag{A.3}$$

Calculating $R$ according to:

$$R = p^3 + q^2, \tag{A.4}$$

the sign of $R$ determines the nature of the roots of Eq. (A.1). When $R>0$, Eq. (A.1) has one real root given by:

$$x_1 = \frac{-a_2}{3} + \sqrt[3]{-q+\sqrt{R}} + \sqrt[3]{-q-\sqrt{R}} \tag{A.5}$$

When $R\leq 0$, Eq. (A.1) has three real roots. When $R=0$, at least two of them coincide. When $R\leq 0$ the roots of Eq. (A.1) can best be calculated according to:

$$x_n = \frac{-a_2}{2} \mp 2.\sqrt{-p}.\cos\left(\frac{\omega + 2n\pi}{3}\right) \quad (\text{with } n = 0, 1, \text{ or } 2) \tag{A.6}$$

with:

$$\omega = \text{Arc}\cos\left(\sqrt{\frac{q^2}{-p^3}}\right) \tag{A.7}$$

In Eq. (A.6), the upper sign applies when $q>0$, the lower if $q<0$.

## References


[1] J.H. Knox, J. Chromatogr. Sci. 7 (1980) 453–461.
[2] G. Guiochon, Anal. Chem. 53 (1981) 1318–1325.
[3] X. Xi, E.S. Yeung, Anal. Chem. 62 (1990) 1580–1585.
[4] A.E. Bruno, E. Grassmann, N. Pericles, K. Anton, Anal. Chem. 61 (1989) 876–883.
[5] J.H. Knox, M.T. Gilbert, J. Chromatogr. 186 (1979) 405–418.

[6] H. Poppe, J. Chromatogr. A 778 (1997) 3.
[7] A.L. Grego, J.C. Díez-Masa, M.V. Dabrio, Anal. Chem. 65 (1993) 1615–1621.
[8] R. Swart, J.C. Kraak, H. Poppe, J. Chromatogr. A 670 (1994) 25–38.
[9] R. Swart, S. Brouwer, J.C. Kraak, H. Poppe, J. Chromatogr. A 732 (1996) 201–207.
[10] K. Göhlin, A. Bushke, M. Larsson, Chromatographia 39 (1994) 729–739.
[11] Y. Guo, L.A. Cólon, Chromatographia 43 (1996) 477–483.
[12] R.P.W. Scott, P. Kucera, J. Chromatogr. Sci. 12 (1974) 453–461.
[13] P.P.H. Tock, P.P.E. Duijsters, J.C. Kraak, H. Poppe, J. Chromatogr. 506 (1990) 185–200.
[14] R.P.W. Scott, J. Chromatogr. 517 (1990) 297–304.
[15] H. Poppe, J.C. Kraak, J. Chromatogr. 225 (1983) 395–414.
[16] D. Schisla, P.W. Carr, Chromatographia 29 (1990) 606.
[17] R. Aris, Proc. Roy. Soc. A252 (1959) 538–550.
[18] R. Swart, J.C. Kraak, H. Poppe, Chromatographia 40 (1995) 587–593.
[19] P.P.H. Tock, C. Boshoven, H. Poppe, J.C. Kraak, J. Chromatogr. 477 (1989) 95–106.
[20] R.P.W. Scott, J. Chromatogr. 468 (1989) 99–114.
[21] J.H. Knox, M. Saleem, J. Chromatogr. Sci. 7 (1969) 614–622.
[22] E.D. Katz, K. Ogan, R.P.W. Scott, J. Chromatogr. Library 32 (1985) 403–434.
[23] E. Katz, K.L. Ogan, R.P.W. Scott, J. Chromatogr. 289 (1984) 65–83.
[24] J.C. Giddings, Anal. Chem. 37 (1965) 60–63.
[25] M. Abramowitz, I. Stegun, Handbook of Mathematical Functions, Dover Publications Inc, New York, 1965.
[26] G. Gujochon, Anal. Chem. 50 (1978) 1812–1821.